



Hydraulic erosion mitigation in sandy soil using cation-crosslinked gelation biopolymer

Minhyeong Lee¹ · Ilhan Chang² · Gye-Chun Cho³

Received: 8 January 2024 / Accepted: 9 February 2025
© The Author(s) 2025

Abstract

The increasing frequency of geotechnical disasters and climate-related land degradation underscores the need of resilient soil erosion mitigation. This study investigates the effectiveness of Cr³⁺-crosslinked xanthan gum (CrXG), a cation-crosslinked gelation biopolymer with time-dependent gelation and water-resistant properties, in mitigating hydraulic soil erosion. Through the erosion function apparatus test, rheological analysis, and microscopic observations, results indicate notable improvements in soil erosion resistance with CrXG treatment, elucidating distinct reinforcing mechanisms attributable to the gel state of the biopolymer hydrogel. The addition of 0.25% CrXG to the soil mass significantly improves critical shear stress and critical velocity, reducing the erodibility coefficient by four order magnitudes compared to untreated sand. Within 48 h, the transition from a viscous to rigid gel state in CrXG, driven by cation crosslinking, transforms the soil from high (II) to low (IV) erodibility class. Scour predictions using the program, based on river hydrograph conditions, indicate a substantial delay in reaching a 1-m scour depth. This study highlights CrXG-soil composite's potential as an advanced geomaterial for mitigating geohazards such as floods and stream scouring, while offering insights into its competitiveness with conventional soil stabilization techniques.

Keywords Chemical crosslinking · Erosion · Erosion function apparatus · Sand · Scouring · Xanthan gum biopolymer

List of symbols

XG	Xanthan gum	τ	Hydraulic shear stress (Pa)
CrXG	Cr ³⁺ -crosslinked XG	V	Flow velocity (m/s)
GG	Gellan gum	τ_y	Rheological yield stress (Pa)
m_b / m_w	The biopolymer-to-water ratio in mass (%)	τ_c	Critical shear stress (Pa)
m_w / m_s	The water-to-soil ratio in mass (%)	v_c	Critical velocity (m/s)
m_b / m_s	The biopolymer-to-soil ratio in mass (%)	k_d	Erodibility coefficient (m/s)
V_p	P-wave velocity (m/s)	θ	Power exponent
\dot{z}	Erosion rate (mm/hr)	c_v	Damping coefficient of viscous-type biopolymer
		c_g	Damping coefficient of gelation-type biopolymer
		k_v	Spring constant of viscous-type biopolymer
		k_g	Spring constant of gelation-type biopolymer

✉ Ilhan Chang
ilhanchang@ajou.ac.kr

✉ Gye-Chun Cho
gyechun@kaist.edu

Minhyeong Lee
leemh@kaeri.re.kr

¹ Disposal Safety Evaluation R&D Division, Korea Atomic Energy Research Institute, Daejeon 34057, Republic of Korea

² Department of Civil Systems Engineering, Ajou University, Suwon-Si 16499, Republic of Korea

³ Department of Civil and Environmental Engineering, Korea Advanced Institute of Science and Technology (KAIST), Daejeon 34141, Republic of Korea

1 Introduction

In recent decades, climate change-induced intense precipitation and rising sea levels have intensified soil erosion challenges, particularly affecting earth structures susceptible to surficial, interfacial, and internal scouring. These

structures, such as bridge abutments, levee slopes, road embankments, and culvert backfills, face risks of catastrophic failure, resulting in fatalities and substantial economic loss. For instance, between 1960 and 1990, stream scour was responsible for 60% of recorded bridge failures in the United States, with annual highway repair costs exceeding \$50 million [46, 78].

To enhance erosion resistance in shallow soil deposits, geotechnical engineers have explored various strategies ranging from soft-to-rigid armoring methods like vegetation [7, 87], rip rap covers [1, 82], and concrete facing [53, 81], to chemical soil stabilization using lime, cement, gypsum, fly ash, and sodium silicate [38, 54, 71, 77]. However, these conventional methods often come with limitations, including high cost, restricted applicability, and potential environmental concerns [24].

As an environmentally conscious alternative, recent investigations have focused on biological approaches, such as microbial- and enzyme-induced calcite precipitation (MICP and EICP) and microbial biofilm formation. Biocementation induces CaCO_3 crystal formation, which increases contact points and surface roughness in coarse soils [20, 34]. This process enhances shear strength and erosion resistance by facilitating interparticle locking [19, 56, 60]. Similarly, microbial biofilms, comprising bacterial cells and extracellular polymeric substances (EPSs), encase soil particles, improving apparent cohesion, reducing permeability, and enhancing erosion resistance [18, 31, 68].

In contrast to endo-cultivated biological stabilization, exo-cultured biopolymer-based soil treatment (BPST) uses mass-produced biopolymers such as xanthan gum (XG), starch, enzymes, and lignin. This approach allows for controlled application and versatile soil stabilization [57]. XG, an anionic, highly viscous extracellular polysaccharide produced by *Xanthomonas campestris*, is particularly noteworthy. XG-based treatments create viscous hydrogels that interact with charged clay surfaces, improving undrained shear strength and enhancing the shear strength of sand-clay mixtures [14, 15, 17]. Its high swelling capacity and pore-filling properties effectively reduce hydraulic conductivity, mitigating seepage and infiltration in granular soils [11, 50]. These properties contribute significantly to erosion resistance across various soil types [26, 44], as demonstrated by multiscale experiments simulating levee overtopping conditions [42, 45].

Despite these benefits, XG's hydrophilic nature limits its durability under prolonged water exposure, leading to soil collapse. To address this, gelation-type biopolymers, such as thermo-gelling and cation-crosslinked biopolymers, have been introduced [48, 83]. While thermo-gelling biopolymers are effective in enhancing strength durability under wet conditions, their field-scale application is

challenging due to the need for precise high-temperature control, affecting workability. In contrast, Cr^{3+} crosslinked xanthan gum (CrXG) offers a straightforward room temperature gelation process [47]. The intermolecular crosslinking between XG's $-\text{COO}$ groups and Cr^{3+} ions gradually increases gel rigidity and reduces water reactivity by consuming hydrophilic sites, forming a robust gel network resistant to long-term submersion [47, 76]. Additionally, CrXG allows control over gelation time through adjustments in biopolymer and Cr^{3+} concentrations, making it highly suitable for field applications. Notably, a 1% CrXG addition to cohesionless sand increased its ultimate bearing capacity by 466% within two days and reduced hydraulic conductivity by four orders of magnitude compared to untreated sand [49].

However, the erosion resistance of CrXG, particularly in both its viscous and stiff gel states under flowing water, remains underexplored. Understanding its surface soil-binding capabilities is crucial for evaluating its effectiveness in protecting against surface and internal erosion in waterfront geotechnical structures. Therefore, this research aims to address these gaps by: (1) characterizing the effects of different gel states on the surface erosion behavior of sand, (2) exploring the mechanisms of soil erosion mitigation through rheological analysis and microscopic observations, and (3) assessing the efficiency and competitiveness of advanced biopolymer treatments.

This study explores the differences in enhancement efficiency and mechanisms between viscous and rigid gel states by investigating the soil erosion resistance, rheological properties, and microscopic structure of biopolymer-treated sand, aiming to assess their effectiveness as erosion mitigation strategies. Specimens treated with non-gelling viscous biopolymers (XG), cation-crosslinked gelation biopolymers (CrXG), and high-temperature gelation biopolymers (gellan gum, GG) were tested under varying hydraulic shear stresses and biopolymer dosage. Soil erosion parameters were measured using an erosion-function apparatus (EFA) and linked to rheological properties to understand erosion mitigation mechanisms depending on biopolymer hydrogel state. Long-term scour predictions using SRICOS software under river hydrograph conditions were also analyzed. This study highlights CrXG's potential as a novel geomaterial for mitigating geohazards like floods and stream scouring, while offering insights into its competitiveness compared to conventional and bio-based soil stabilization techniques.

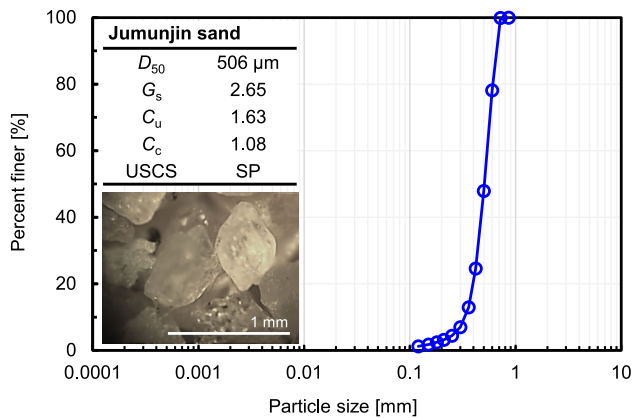


Fig. 1 Grain size distribution and basic properties of jumunjin sand

2 Materials and methods

2.1 Soil

Jumunjin sand, a commonly used silica sand in Korea, was selected as the host soil for this study. Classified as poorly graded sand (SP) according to the Unified Soil Classification System (USCS), it has a mean particle size (D_{50}) of 0.506 mm. The particle-size distribution curve and detailed soil properties are illustrated in Fig. 1. Based on the erosion classification in Briaud (2008), SP soil falls between “very high erodibility” and “high erodibility”.

2.2 Biopolymer: hydrogel preparation

Three biopolymers—XG, CrXG, and GG—were considered for hydrogel preparation and subsequent mixing with

soil. XG, known for its non-gelling yet highly viscous nature in water, strengthens soil through interparticle bonding [14] and reduces hydraulic conductivity via pore filling effects [11]. Analytical grade purified XG powder (Sigma-Aldrich, CAS: 11,138–66-2) was used to prepare XG hydrogels, with biopolymer mass-to-water mass ratio (m_b/m_w) of 0.625%, 1.25%, 2.5%, and 5% using a laboratory hand mixer.

CrXG, a crosslinked form of XG with Cr^{3+} cations, is recognized for its rapid improvement in wet strength and mitigation of water infiltration in coarse soils through progressive gelation. Additionally, CrXG shows enhanced durability against water-related degradation [47]. The synthesis of CrXG gel involved combining XG hydrogel with a Cr^{3+} solution, made from chromium nitrate non-hydrate ($\text{Cr}(\text{NO}_3)_3 \cdot 9\text{H}_2\text{O}$) and sodium chloride (NaCl) in distilled water. $\text{Cr}(\text{NO}_3)_3 \cdot 9\text{H}_2\text{O}$ (Daejung Chemical Co., CAS: 7789-02-8) was chosen as the crosslinking agent due to its high solubility and effective crosslinking reactivity among Cr^{3+} compounds [5, 36]. The m_b/m_w ratio for CrXG gel were set at 0.625%, 1.25%, 2.5%, and 5%. The final mixing ratio of XG: $\text{Cr}(\text{NO}_3)_3 \cdot 9\text{H}_2\text{O}$:NaCl by mass was maintained at 10:3:1, following the previous findings that reported this mixing ratio as optimal for wet strength performance [47].

GG, a thermogelation biopolymer synthesized by the bacterium *Sphingomonas elodea*, exhibits changes in thickness and solubility with temperature variation. When heated above 110 °C in water, GG undergoes an ionotropic sol–gel transition upon cooling, forming a dense and highly viscoelastic gel that contributes to increased soil shear strength [12]. Low acyl GG (Sigma-Aldrich, CAS No:

Table 1 Description of soil specimens

Specimen number	Specimen name (Label)	Biopolymer type (Binder)	Binder content to soil mass (m_b/m_s) [%]	Initial water content (m_s/m_w) [%]	Concentration of binder gel (m_b/m_w) [%]	Dry density [g/cm^3]	Void ratio	Relative Density [%]
1	Untreated	–	–	20	–	1.45	0.83	39
2	X12	Xanthan gum	0.125		0.625	1.44	0.84	35
3	X25	(XG)	0.25		1.25	1.46	0.82	44
4	X50		0.5		2.5	1.45	0.83	39
5	X100		1		5	1.44	0.84	35
6	CX12	Cr^{3+} -crosslinked Xanthan gum	0.125		0.625	1.47	0.80	48
7	CX25	(CrXG)	0.25		1.25	1.43	0.85	31
8	CX50		0.5		2.5	1.44	0.84	35
9	CX100		1		5	1.44	0.84	35
10	CX12(48 h)		0.125		0.625	1.47	0.80	48
11	CX25(48 h)		0.25		1.25	1.46	0.82	44
12	GG25	Gellan gum	0.25		1.25	1.46	0.82	44
13	GG50	(GG)	0.5		2.5	1.48	0.79	51
14	GG100		1		5	1.44	0.84	35

71010–52-1) was used to prepare GG solutions with m_b/m_w ratio of 1.25, 2.5, and 5%, achieved by dissolving the powder in distilled water heated to 110 °C [12].

2.3 Biopolymer-treated soil column preparation

A series of biopolymer-treated soil column specimens were prepared for the flume-type erosion tests (Table 1) using the wet-mixing method, where the hydrogel was prepared first and then mixed with soil to improve workability and ensure mixing homogeneity in biopolymer-soil composite [14, 74]. Jumunjin sand, dried at 110 °C for 24 h, was thoroughly mixed with XG, CrXG, and GG hydrogels to achieve an initial water content (m_w/m_s = water mass in hydrogel-to-soil mass ratio) of 20%. This process produced biopolymer-treated sand with biopolymer-to-soil mass ratio (m_b/m_s) of 0.125%, 0.25%, 0.5%, and 1%. The mixtures were compacted into Shelby tubes (inner and outer diameters of 71 mm and 76.2 mm, respectively), resulting in soil columns with a height of 200 mm and an initial void ratio ranging from 0.79 to 0.85, which corresponds to a dry density (ρ_d) range of 1.43 to 1.48 g/cm³. The upper surface of the column was carefully trimmed, and both ends of the tube were sealed with paraffin film to prevent moisture evaporation prior to conducting experiments. A total of 14 specimens were prepared, as summarized in Table 1.

According to Marudova-Zsivanovits et al. (2007), the gelation process in XG-Cr³⁺ gel can be divided into two phases: the initial 12 h, referred to as the *rising* period, during which the gel stiffness increases, and the subsequent 48 h, known as the *plateau* period, during which the gel stiffness remains constant. Because of this, the CrXG hydrogel specimen was divided into two types based on the curing time: early-stage and post-gelation. The early stage CrXG specimens (No. 6, 7, 8 and 9), which were closer to the viscous gel state, experienced early-stage gelation lasting a maximum of 6 h. This period encompassed the entire timeframe from specimen preparation to the conclusion of the erosion test. In contrast, the post-gelation CrXG specimens (No. 10 and 11) were pre-cured for 48 h prior to the erosion test. The curing effect was not considered for the viscous XG (No. 2, 3, 4 and 5) and thermogelated GG specimens (No. 12, 13 and 14), as they did not experience gelation over time. In summary, specimens from No. 2 to No. 9 contained a viscous biopolymer hydrogel, whereas specimens from No. 10 to No. 14 included a rigid biopolymer hydrogel.

2.4 Erosion test using erosion function apparatus (EFA)

To assess surface erosion resistance of biopolymer-treated soil specimens, an erosion function apparatus (EFA)

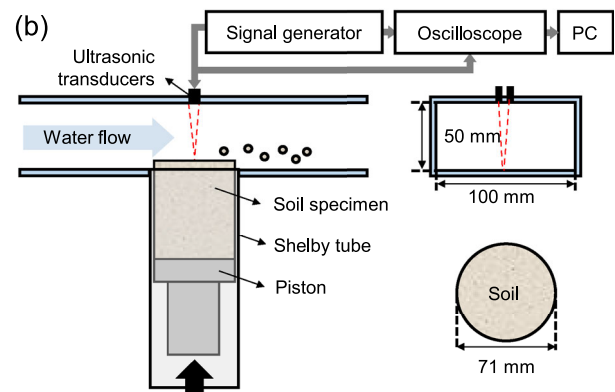
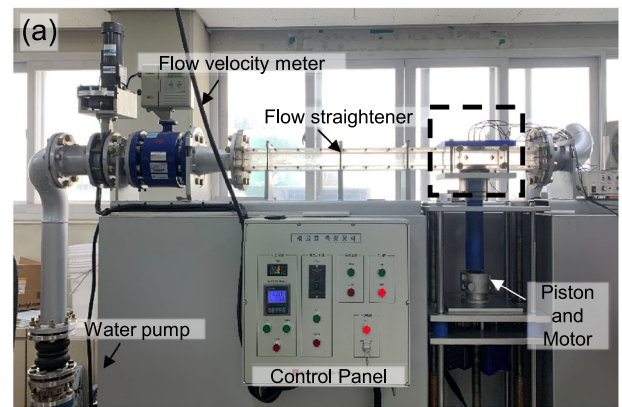


Fig. 2 Erosion function apparatus (EFA) used in this study: **a** configuration of EFA, and **b** specimen and P-wave monitoring system in conduit

equipped with a P-wave monitoring system was employed (Fig. 2) [10, 33]. Specimens were placed into the EFA (Fig. 2a), with the upper portion of each specimen threaded through the lower opening of the conduit. Once the conduit was filled, a pneumatic piston raised the soil columns to protrude 1 mm into the conduit's lower surface (Fig. 2b). These columns were then subjected to water flow velocities ranging from 0.07 to 4.87 m/s, representing the EFA's operational limits.

Erosion time (t), defined as the duration of water exposure required to produce 1 mm soil erosion, was measured through visual inspection and P-wave reflection monitoring. Two pencil-type miniature ultrasonic transducers (VP-3, CTS Valpey Co.) with a 3 mm diameter were affixed to the upper center of the flow channel. During testing, a signal generator (DPR300, JSR Ultrasonics) produced pulses on the source transducer, while reflected P-waves were captured by the receiver transducer every 3 s using a digital oscilloscope (DSO-X-3024A, Agilent) (Fig. 3). Data processing involved applying a band-pass filter with cutoff frequencies between 1.5 and 4.0 MHz to improve signal clarity. The eroded height (Δz , in mm) was

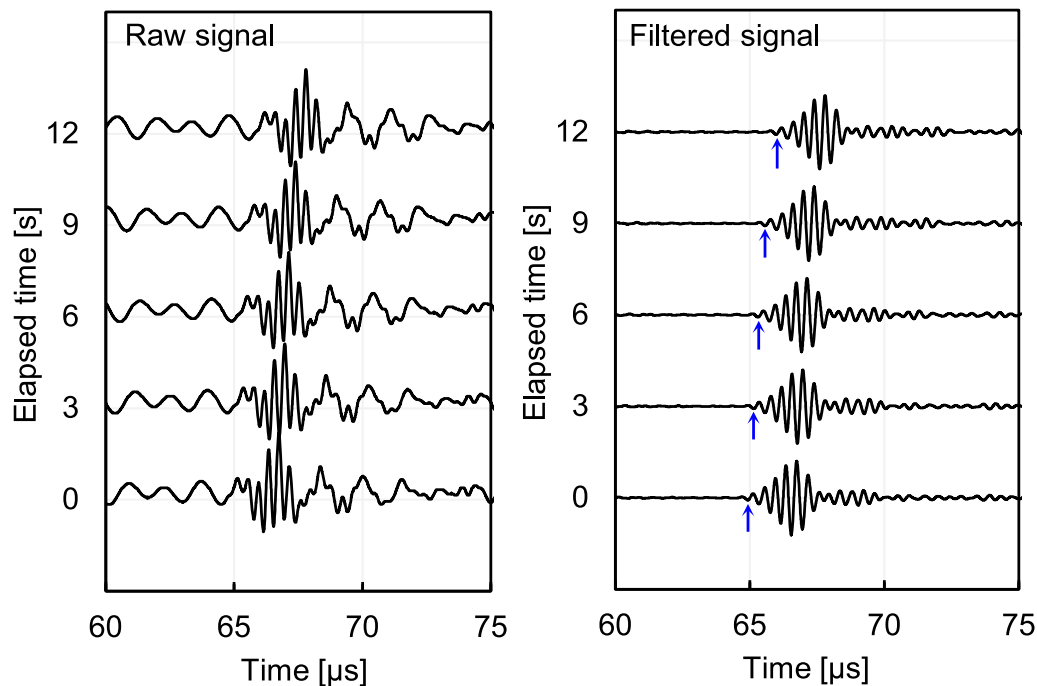


Fig. 3 Raw and filtered P-wave signals in EFA test

then calculated based on the change in arrival time (Δt_p , in s) and the P-wave velocity in water (V_p , 1480 m/s at 20 °C) as follows [33]:

$$\Delta z = \frac{1}{2} V_p (\Delta t_p) \quad (1)$$

Figure 4 depicts soil depth variation at the central location of the soil specimen as estimated through P-wave reflection monitoring under different flow velocities during the EFA tests. The t was determined by averaging the time at which soil depth change exceeded 1 mm with the time recorded from visual inspection (Fig. 4a). In cases where air bubbles interfered with P-wave signals [33], only visual inspection was used to record t . When surface erosion was minimal but specimen fragments dislodged at higher flow velocity, t was recorded at the time of fragment detachment (Fig. 4b). For specimens with negligible erosion even after one hour, t was set at 3600 s (Fig. 4c).

The EFA method analyzes soil erosion behavior through erosion rate (\dot{z} , in mm/h) and shear stress (τ , in Pa). The \dot{z} was calculated by dividing the eroded depth by the time needed for 1 mm erosion (t) as follows [10]:

$$\dot{z} = \frac{1}{t} \times 3600 \quad (2)$$

Shear stress in the EFA was determined using the Darcy-Weisbach equation as a function of flow velocity (V), density of water (ρ) and friction factor (f) [35]:

$$\tau = \frac{1}{8} f \rho V^2 \quad (3)$$

The Moody chart, modified for the rectangular pipe, provided the friction factor as a function of pipe roughness (ϵ) and the Reynolds number (Re) [61].

2.5 Measurement of rheological yield stress of biopolymer hydrogels

Shear-thinning biopolymer hydrogels exhibit a reduction in viscosity when subjected to an external shear force exceeding the rheological yield stress (τ_y) [80]. τ_y , which is stress required to initiate flow or disrupt the integrity of a gel structure, was measured using a rheometer (Rheolab QC, Anton Paar) equipped with a 4-blade vane spindle. For biopolymer hydrogels in a viscous state (e.g., XG and early-stage CrXG gels in specimens No. 2 to No. 9), a shear rate of 0.05 s^{-1} were applied, and τ_y was calculated using Eq. (4) as shown below [27]:

$$\tau_y = \frac{2}{\pi D^3} \left(\frac{H}{D} + \frac{1}{3} \right)^{-1} T_{\max} \quad (4)$$

where τ_y = yield stress (Pa); D = vane width (m); H = vane height (m); and T_{\max} = maximum torque (N·m).

Due to the excessively high τ_y and stiffness of the gelation type biopolymer hydrogels (specimen No. 10 to No. 14), which make rheometer measurement impractical, only viscous state biopolymers were evaluated.

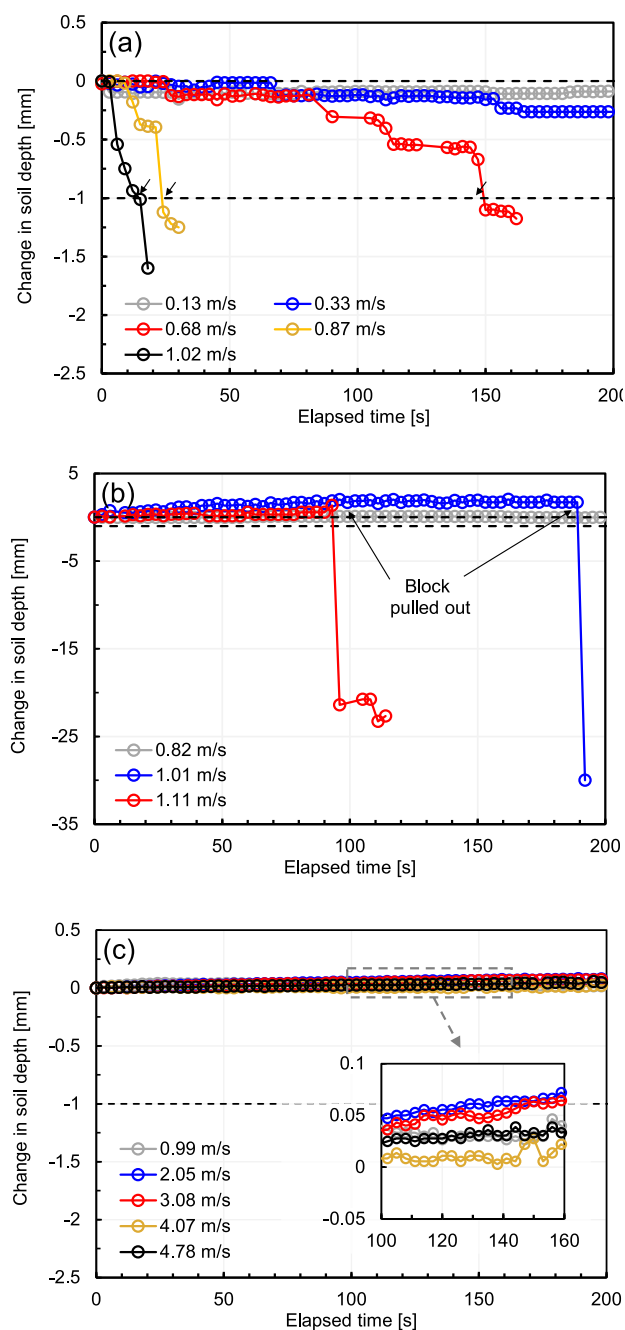


Fig. 4 Change in soil depth obtained by P-wave reflection monitoring: **a** X25; **b** CX50; and **c** CX25 (48 h)

2.6 Microscopic observations of biopolymer-treated sand

Environmental scanning electron microscope (ESEM) analysis was conducted using a Quattro S (Thermo Fisher Scientific Inc.) to observe the microscopic structure of viscous- and gelation-type biopolymer hydrogels within a sand matrix under humid conditions. A piece of XG- and CrXG-treated sand specimen was mounted on a circular

ESEM stage and exposed to electron beams in a chamber maintained at 100% relative humidity by controlling the water vapor pressure at 750–770 Pa and the temperature at 2 °C.

2.7 SRICOS-EFA

The *Scour Rate in Cohesive Soil* (SRICOS) method, introduced by Briaud et al. (1999), predicts scour depth over time using hydrograph data and erosion function (τ – z relations) derived from EFA experiments. This method was employed to evaluate the effectiveness of biopolymer-soil treatments in scour mitigation, with further details outlined in Briaud et al. (2001). A simplified scenario was modeled with three circular piers in the *Seomjingang* River, an area severely affected by flooding in 2020 in Korea [65]. The modeled river segment has a stream width of 130 m (Fig. 5a). The riverbed was simulated with two layers: an upper 1 m-thick layer treated with biopolymer-soil, and a lower 9 m-thick layer of untreated soil (Fig. 5b). Hydrograph data (discharge in m^3/s) from 2004 to 2022 for *Seomjingang* River in Gokseong-gun, Jeollanam-do, Korea, was obtained from the Water Environment Information System of Korea [62], as depicted in Fig. 6. Over the 19-year period, discharge fluctuated significantly due to seasonal heavy rainfall, with a mean discharge of $26.5 \text{ m}^3/\text{s}$, a peak discharge of $4906 \text{ m}^3/\text{s}$ in August 2020, and a standard deviation of $107 \text{ m}^3/\text{s}$.

3 Results and analyses

3.1 Effect of biopolymer treatment on erosion time under variable water flow condition

Figure 7 shows the time required to achieve 1 mm erosion in untreated sand and sand treated with the three different biopolymers across varying flow velocities (detailed data are available in Table S1). The solid gray line at $t = 3600 \text{ s}$ represents cases where a minimal erosion ($< 1 \text{ mm}$) occurred within 1 h. Figure 8 contrasts surface erosion behavior between untreated sand and CX12(48 h).

For the untreated sand (Fig. 7a), minimal erosion was observed at flow velocities (V) of 0.07 to 0.10 m/s, with a significant erosion initiating at $V = 0.11$ to 0.16 m/s. These findings align with previous findings (V ranging from 0.1 to 0.2 m/s) [33, 44] and suggest that untreated jumunjin sand, prone to erosion under water flow, is vulnerable at velocities common during rainfall (0.05 to 0.30 m/s) on slope and along rivers 0.4 to 1.5 m/s [73, 86], untreated jumunjin sand is prone to erosion under water flow.

Biopolymer-treated sand demonstrated greater resistance to erosion compared to untreated sand, with

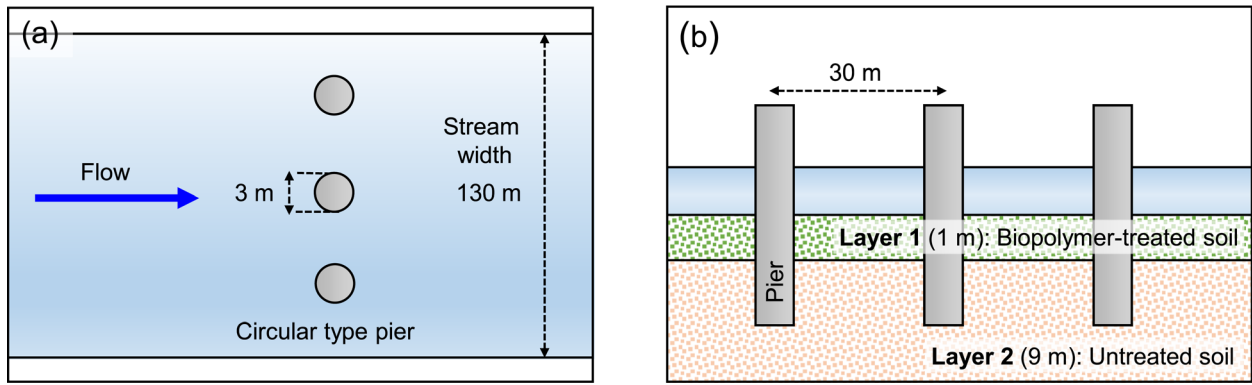


Fig. 5 Geometry of the piers and stream channel for SRICOS prediction

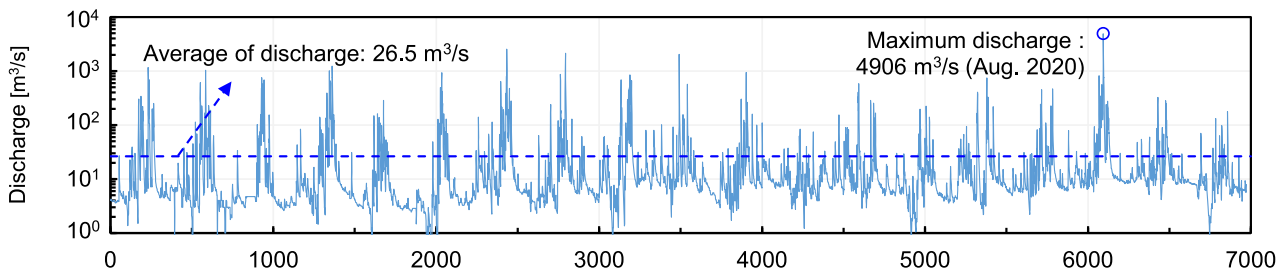


Fig. 6 Hydrograph of Seomjingang River from 2004 to 2022

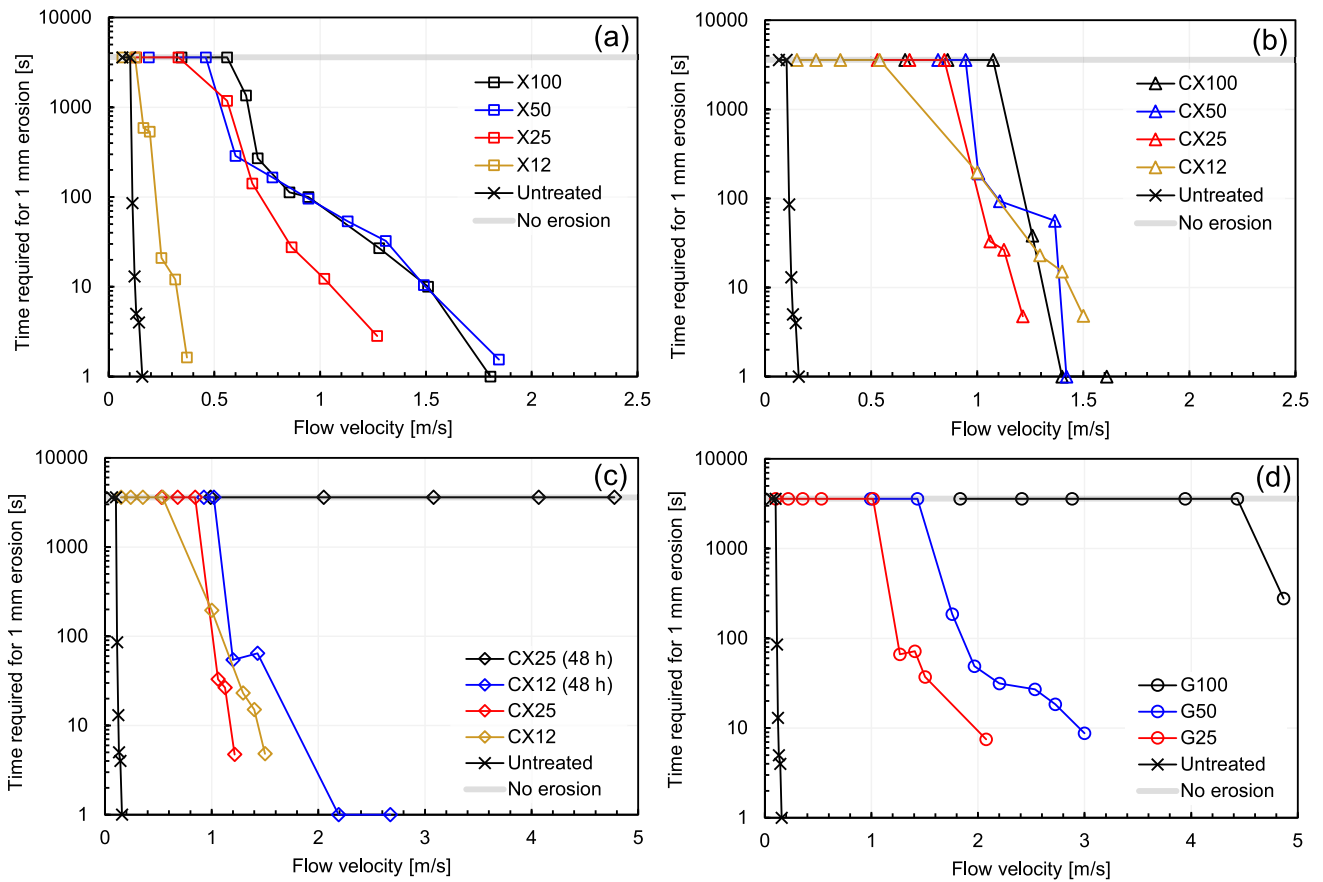


Fig. 7 Time required for 1 mm erosion by surficial flow velocity: a XG; b CX; c Cured CX; and d GG

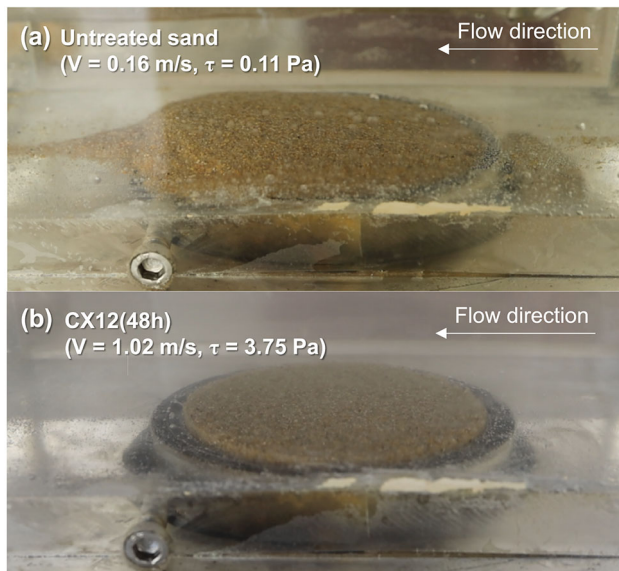


Fig. 8 Observed erosion behavior: **a** untreated sand at $V = 0.16$ m/s, and **b** CX12(48 h) at $V = 1.02$ m/s

variations depending on biopolymer type and dosage (m_b/m_s). Untreated sand exhibited rapid erosion rapidly at $V = 0.16$ m/s (Fig. 8a), while minimal XG treatment ($m_b/m_s = 0.125\%$) extended erosion time to 590 s at $V = 0.17$ m/s (Fig. 7a). Increasing the XG dosage to 1% further delayed erosion, extending erosion times beyond 1000 s at $V = 0.4$ – 0.7 m/s, showcasing enhanced erosion resistance with higher XG viscosity. However, for all XG-treated soils, erosion still initiated below $V = 1$ m/s.

In contrast, early-stage Cr^{3+} crosslinking-induced XG gelation in CrXG-treated sand showed minimal erosion at $V < 1$ m/s (Fig. 7b), attributable to partial thickening by localized bonding between COO^- groups and Cr^{3+} ions during gel mixing [64]. At $V = 1$ – 1.5 m/s, XG and CrXG exhibited similar erosion times (under 100 s at $m_x/m_s = 0.5\%$ and 1%), likely due to the shear-thinning properties of both hydrogels [23]. This indicates that adding Cr^{3+} delays erosion onset in XG-treated sand, but without significant variation in erosion time once erosion begins, as the shear force disrupts further intermolecular bonding [23].

CrXG-treated sand cured for 48 h (Fig. 7c) showed substantially increased erosion resistance compared to the early stage gelation. Erosion time increased from 195 s (CX12) to 3600 s (CX12(48 h)) at $V = 1.0$ m/s (Fig. 8b). CX12(48 h) required twice the flow velocity to initiate erosion compared to CX12, and CX25(48 h) remained intact at $V = 4.8$ m/s. This enhanced erosion resistance is attributed to the transition of CrXG hydrogel from a high-viscosity to high-rigidity state, strengthening the gel network through bonding between XG molecules and Cr^{3+}

[29], thereby limiting deformation and improving the erosion resistance of the soil.

GG-treated sand (Fig. 7d), which transitions to a rigid gel upon heating (110 °C) and subsequent cooling, exhibited erosion resistance comparable to that of 48-h cured CrXG-treated sand. Unlike XG-treated sand, GG-treated specimens at m_b/m_s of 0.25%, 0.5%, and 1% exhibited erosion times of 8, 49, and 3600 s, respectively, even at $V = 2$ m/s. GG-treated sand with m_b/m_s of 1% showed minimal erosion, similar to 48-h cured CrXG-treated specimens, until reaching $V \approx 4.5$ m/s.

3.2 Effect of biopolymers on erosion rates and erosion resistance parameters

Critical shear stress (τ_c), defined as the maximum hydraulic stress (τ) required to initiate erosion, and critical velocity (v_c), the maximum velocity that soil can withstand without eroding, are key parameters for assessing soil erodibility. To analyze the effect of biopolymer treatment on soil erodibility, τ_c and v_c were determined using a $\dot{z} - \tau$ plot on log–log scale. An erosion rate threshold of 1 mm/h was set on the y-axis, with τ_c (and v_c) identified as the average of the last τ value where $\dot{z} = 1$ and the first τ value where $\dot{z} > 1$ [31, 75]. Erosion curve were modeled based on a power relationship between z and $\tau - \tau_c$ (excess shear stress) as follows [40, 84]:

$$\dot{z} = k_d \left(\frac{\tau - \tau_c}{1 \text{ Pa}} \right)^\theta \quad (5)$$

where k_d is the erodibility coefficient (mm/hr), indicating the sensitivity of \dot{z} to shear stress increment, τ_c is the critical shear stress (Pa), and θ is the power exponent describing the curve shape related to the erosion mode. Due to minimal erosion observed in the CX25(48 h) even at the maximum flow velocity in EFA (~ 4.8 m/s), erosion parameters for CX25(48 h) could not be determined by conventional method, so a maximum shear stress of 80.5 Pa was used as τ_c for subsequent analysis. The erosion parameters are summarized in Table 2 based on Briaud (2008) erosion category chart.

Figure 9 shows erosion curves for untreated and biopolymer-treated sand. Untreated sand, categorized as ‘very high erodibility (I)’, exhibited a τ_c of 0.06 Pa, v_c of 0.11 m/s, and k_d of 386,290 mm/hr (Fig. 9a). While \dot{z} reached 42 mm/h at τ of 0.11 Pa for untreated sand, all biopolymer-treated sands showed significantly reduced \dot{z} at comparable τ levels. Viscous biopolymer hydrogels, XG and early stage CrXG, increased τ_c up to 1.40 Pa and 5.03 Pa (v_c up to 0.61 m/s and 1.17 m/s) at $m_b/m_s = 1\%$, moving erodibility class to ‘high erodibility (II)’ (Fig. 9b). The difference in effectiveness between XG and CrXG

Table 2 Summarized EFA test results: erosion parameters and erosion category

Specimen	Flow velocity v [m/s]	Shear stress \dot{z} [Pa]	Critical velocity v_c [m/s]	Critical shear stress τ_c [Pa]	Erodibility coefficient k_d [mm/hr]	Power exponent θ [-]	Erosion category adopted from Briaud (2008)
Untreated	0.07 ~ 0.16	0.02 ~ 0.11	0.11	0.05	386,290	1.74	Very high (I)
X12	0.07 ~ 0.37	0.02 ~ 0.57	0.15	0.10	5031	1.95	Very high (I)
X25	0.13 ~ 1.27	0.08 ~ 5.89	0.45	0.82	29	2.44	High (II)
X50	0.19 ~ 1.85	0.16 ~ 12.3	0.53	1.10	28	1.26	High (II)
X100	0.35 ~ 1.81	0.48 ~ 11.7	0.61	1.40	26	1.55	High (II)
CX12	0.15 ~ 1.50	0.10 ~ 8.16	0.77	2.41	10	2.28	High (II)
CX25	0.54 ~ 1.22	1.12 ~ 5.40	0.95	3.40	172	1.68	High (II)
CX50	0.82 ~ 1.42	2.48 ~ 7.33	0.98	3.52	85	1.25	High (II)
CX100	0.66 ~ 1.61	1.65 ~ 9.38	1.17	5.03	254	2.20	High/medium (II-III)
CX12(48 h)	0.93 ~ 2.68	3.17 ~ 27.3	1.11	4.52	47	1.40	High/Medium (II-III)
CX25(48 h)	1.00 ~ 4.78	3.62 ~ 80.5	4.78	> 80.5	N/A ^a	N/A	Low (IV)
GG25	0.10 ~ 2.08	0.05 ~ 15.5	1.14	4.84	37	0.98	High/Medium (II-III)
GG50	0.99 ~ 3.00	3.64 ~ 32.0	1.60	9.31	12	1.05	Medium (III)
GG100	1.83 ~ 4.87	12.1 ~ 83.7	4.65	76.6	N/A	N/A	Medium/Low (III-IV)

^a N/A = Not available for erosion curve fitting due to negligible erosion

stems from initial gel thickening due to intermolecular bonding during CrXG gel mixing, as discussed in Sect. 3.1.

CrXG-treated sand cured for 48 h exhibited even higher τ_c and v_c values due to enhanced gelation (Fig. 9c). CX12(48 h) shifted to ‘high-to-medium erodibility (II-III)’, and CX25(48 h) to ‘low erodibility (IV)’. GG-treated sand showed similar improvements, reaching τ_c of 9.31 Pa ($v_c = 1.60$ m/s) at $m_b/m_s = 0.5\%$, positioning the erosion curve in ‘medium erodibility (III)’ category (Fig. 9d).

3.3 Effect of biopolymer content on the efficiency of erosion resistance improvement

To evaluate the effect of biopolymer content on erosion resistance efficiency, Fig. 10 presents normalized erosion resistance parameters (Table 3). Experimental results confirmed that increasing m_b/m_s improves τ_c and v_c across all biopolymer types (Fig. 10a, b). Reductions in k_d were less pronounced but showed decreases of 3 to 4 magnitudes compared to untreated sand (Fig. 10c), consistent with findings by Kwon et al. (2020). Cr^{3+} crosslinking-induced gelation significantly increased improvement efficiency, with XG treatment showing efficiency increases from 1.7 to 15 for τ_c (and 1.4 to 4.2 for v_c) as m_b/m_s rose from 0.125 to 0.25%. In contrast, 48-h cured CrXG treatment showed a higher efficiency increase, from 82 to 1467 (and 10 to 45 for v_c). This difference is attributed to the continuous

crosslinking in XG- Cr^{3+} gel network, which restricts deformation and increases structural strength. Higher XG content also enhances improvement efficiency by providing more active crosslinking sites and reducing branch distances, promoting faster gelation and stronger gels [67]. Additionally, CrXG treatment achieves similar improvements with only a quarter of the GG biopolymer content, aligning with previous studies comparing the unconfined compressive strength and direct shear cohesion of CrXG- and GG-treated sands [49].

4 Discussions

4.1 Mechanism of enhancement in viscous- and gelation-type biopolymers

Saturated soil particles are detached at fluid-particle interfaces through lifting and drag forces [52]. Experimental findings indicate that adding viscous- and gelation-type biopolymers increases soil resistance to water flow by raising the energy required for erosion, which involves breaking interparticle bonds and achieving full suspension in the flow [38]. Three possible mechanisms contribute to this enhancement: (1) acting as a viscous fluid damper, (2) serving as a bonding bridge to enhance interparticle contact, and (3) filling pores to reduce seepage-induced erosional forces. Figure 11 provides a conceptual schematic

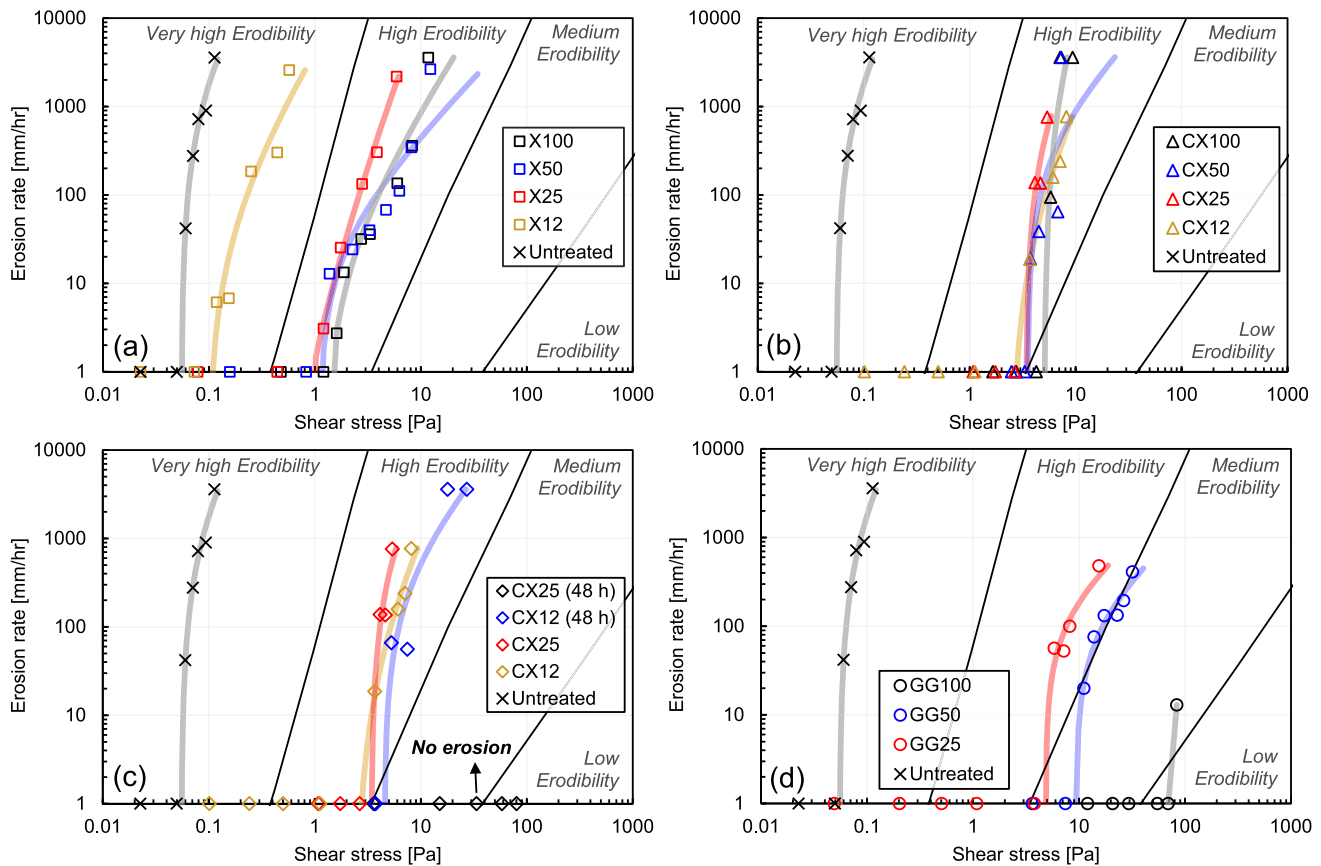


Fig. 9 Erosion curve of viscous- and gelation-type biopolymer-treated sand: **a** XG; **b** CX; **c** Cured CX; and **d** GG

illustrating the role of viscous- and gelation-type biopolymer hydrogels in the soil matrix under water flow. Using a spring-dashpot system (Kelvin-Voigt model) as an analogy, the viscoelastic behavior of pore-filling biopolymer hydrogels is represented, with distinct differences in spring constants and damping coefficients (i.e., $c_v > k_v$ for viscous hydrogels, and $c_g < k_g$ for gelation-type hydrogels) [22, 63]. Figure 12 presents ESEM images of viscous (XG) and gelation-type (CrXG) biopolymer-treated sand specimens under humid conditions (relative humidity = 100%).

In its initial viscous hydrogel state, XG hydrogel displays negligible tensile strength. As it dehydrates beyond 20% m_b/m_w , XG hydrogel transitions to a rigid film with a tensile strength of approximately 5 MPa (Fig. S1a) [37]. This explains why no significant increase in peak shear strength or cohesion intercept is observed for XG-treated sand in its initially wet state during direct and triaxial tests, as XG chains lack direct interaction with electrostatically neutral sand particles [37, 51]. However, viscous XG-treated sand demonstrates increased ductility, indicating that greater strain energy is required for failure compared to untreated sand [49]. In this context, the presence of a viscous fluid (Fig. 12a), characterized by a relatively high

c_v and low k_v , within the sand's pore likely impedes particle movement (deformation) and dissipates excess energy, acting as a viscous damper rather than providing tensile strength through interparticle bonding (Fig. 11a).

Figure 13 illustrates the relationship between τ_c of sand treated with viscous gel-type biopolymers (XG and early stage CrXG) and τ_y of the viscous biopolymer hydrogel (Table 4). This τ_y represents the critical point at which the hydrogel loses its damping effect. The τ_c of the treated sand shows a proportional increase with the τ_y of the treating hydrogel (for $\tau_y > 3.38$ Pa) in a logarithmic relationship, expressed as:

$$\tau_c = 0.87 \ln(\tau_y) - 1.06 (R^2 = 0.86) \quad (6)$$

This finding supports the hypothesis that the viscous biopolymer hydrogel loses its damping effects as its storage modulus decreases, especially when flow-induced stress exceeds the hydrogel's τ_y , ultimately leading to the loss of particle-holding particles.

In contrast, GG and 48-h cured CrXG hydrogels in a rigid gel state exhibit tensile strength even in a wet state (Fig. S1b) [13, 47]. Coating particles with these rigid hydrogels, characterized by relatively low c_v and high k_v , forms bonding bridges (Fig. 11b), as observed in ESEM

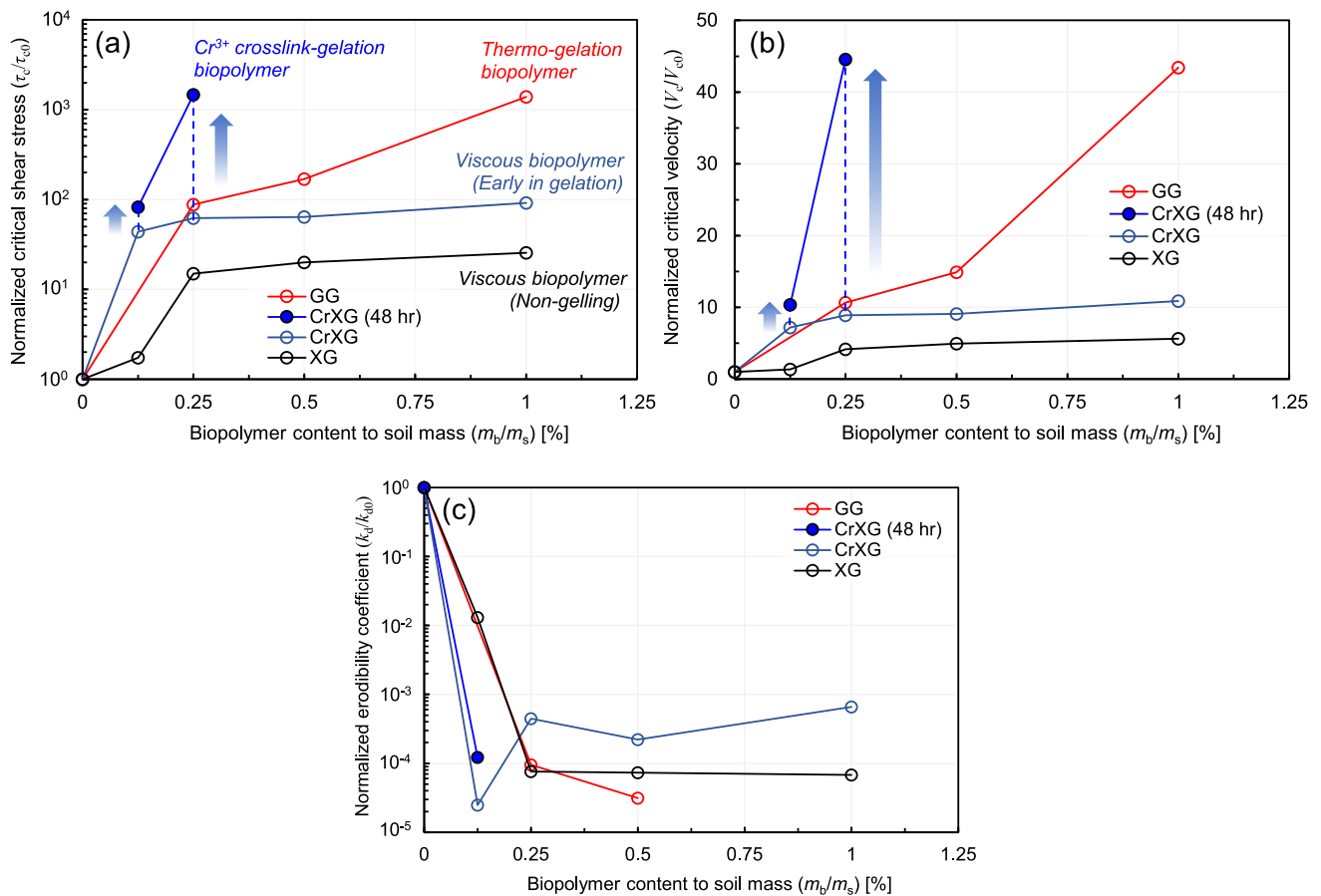


Fig. 10 Variations in normalized erosion resistance parameters by biopolymer gel state and content: **a** critical shear stress, **b** critical velocity, and **c** erodibility coefficient

images (Fig. 12b). This increases particle contacts and requires additional shear stress cycles (energy) to break them. Furthermore, the formation of sand-biopolymer aggregates likely increases the mean grain size, which is proportional to the critical shear stress of non-cohesive soils, thereby increasing the energy required to suspend eroded particles [10].

Finally, the pore-filling effect in both viscous- and gelation-type biopolymer hydrogels restricts seepage flow, reducing soil permeability through pore clogging [31]. The improved strength durability of gelation-type biopolymer-treated sand during water infiltration, due to its reduced water reactivity, also supports its superior erosion resistance compared to viscous biopolymers [47]. Consequently, the combined effect of inhibited particle displacement and reduced infiltration results in an increased τ_c and a decreased k_d value.

4.2 Competitiveness of CrXG treatment for erosion mitigation

4.2.1 Comparison with other bio-based soil improvement methods

The effectiveness of CrXG treatment in enhancing τ_c was compared with various bio-based soil improvement methods previously evaluated through EFA tests (Fig. 14). Bio-based techniques include exo-cultivated methods, such as direct mixing of biopolymers, enzymes, and lime [43, 75, 77], and endo-cultivated methods, like MICP and EPS formation, which introduce liquid inoculum into the soil medium [31, 32, 70]. Results indicate that most bio-based methods achieve at least a two-fold increase in τ_c for sandy soils compared to untreated soil. However, EPS and MICP demonstrate relatively modest improvements due to difficulties in achieving homogeneous distribution and substantial treated volume with endo-cultivation methods [19]. In contrast, XG and XG-based compound biopolymer treatments yield substantial increases in τ_c , ranging from 2 to 28 times that of untreated sand.

Table 3 Normalized erosion resistance parameters of untreated and biopolymer-treated soil

Specimen	Normalized erosion parameter [-]		
	v_c/v_{c0}^a	τ_c/τ_{c0}	k_d/k_{d0}
Untreated	1	1	1
X12	1.4	1.7	1.3×10^{-2}
X25	4.2	15	7.6×10^{-5}
X50	4.9	20	7.3×10^{-5}
X100	5.6	26	6.8×10^{-5}
CX12	7.2	44	2.5×10^{-5}
CX25	8.9	62	4.5×10^{-4}
CX50	9.1	64	2.2×10^{-4}
CX100	11	92	6.6×10^{-4}
CX12 (48 h)	10	82	1.2×10^{-4}
CX25 (48 h)	45	1467	N/A
GG25	11	88	9.5×10^{-5}
GG50	15	170	3.1×10^{-5}
GG100	43	1395	N/A

^a v_{c0} , τ_{c0} , and k_{d0} are critical velocity, critical shear stress, erodibility coefficient for untreated sand, respectively

These findings establish XG-based soil treatment as a viable solution for mitigating both surface and internal erosion in levee structures, as demonstrated in a large-scale experiment [42, 45]. Furthermore, CrXG treatment provides significantly improvement in τ_c over to untreated sand, with over 100-fold enhancement relative to XG alone, driven by the transition from a viscous to a rigid gel. Lime, a conventional soil stabilizer, raises τ_c in sandy soil from 0.52 to 1.2 Pa after 7 days of curing, increasing further to 114 Pa after 28 days through hydration. Although the final τ_c of CrXG-treated soil may be lower than that achieved by cementitious materials post-complete

hydration, CrXG biopolymer treatment offers distinct early-stage construction benefits, enabling rapid reinforcement and temporary erosion mitigation in soil applications.

4.2.2 Scouring depth prediction

The erosion resistance observed in the EFA experiments was assessed under controlled conditions with constant flow velocities, which may not fully reflect the variability in flow conditions caused by seasonal changes in natural environment (Fig. 6). To address this, SRICOS software was used to predict scour depth and evaluate the performance of biopolymer-soil treatments under variable flow velocities, providing a more realistic representation of riverbed dynamics.

Figure 15 shows the predicted scour depth over 19 years for *Seomjingang* river, accounting for variations in discharge, water velocity, and depth. Significant increases in scour depth were noted during periods of seasonal heavy rainfall, particularly on days 247, 2448, and most notably 6094, when discharge peaked at 185 times the average, corresponding to the major flood event in August 2020. For untreated soil, the time to reach a 1-m scour depth was 173 days. Biopolymer treatments showed effective mitigation of scouring around piers, with XG treatment extending the time to reach a 1-m scour depth by factors of 1.3 to 7.9, depending on the m_b/m_s . CrXG treatment demonstrated superior performance, delaying the 1-m scour depth by up to 35 times. After 19 years, the final scour depth for both untreated and viscous-type biopolymer-treated soils was 5.24 m, whereas gelation-type biopolymer-treated soils showed a 31% reduction in final scour depth (3.61 m) even after the extreme flood event. Due to curve-fitting issues in SRICOS, the CX25(48 h) treatment, which demonstrated the highest erosion

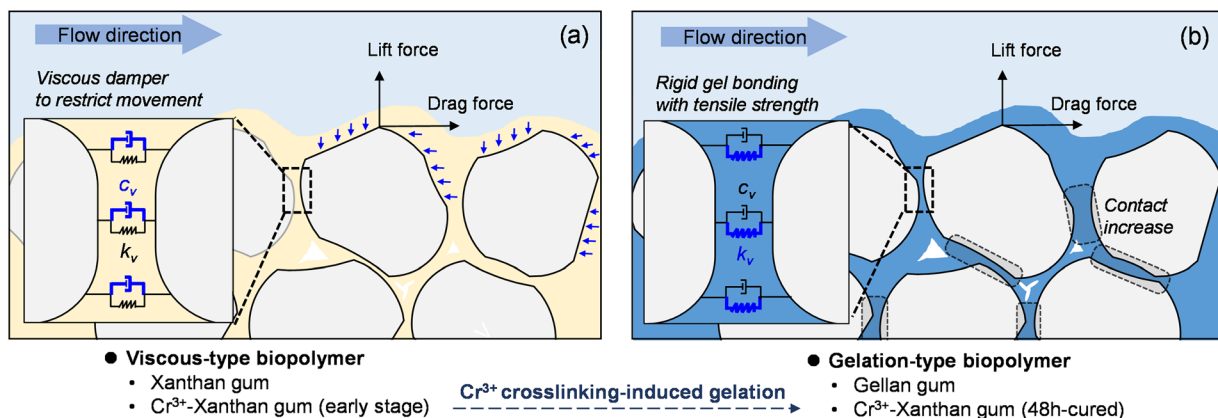


Fig. 11 Schematic for the erosion mitigation mechanism of biopolymer in sand: **a** viscous-type, and **b** gelation-type. c_v and c_g denote the damping coefficient, k_v and k_g denote spring constant of viscous- and gelation-type biopolymer, respectively

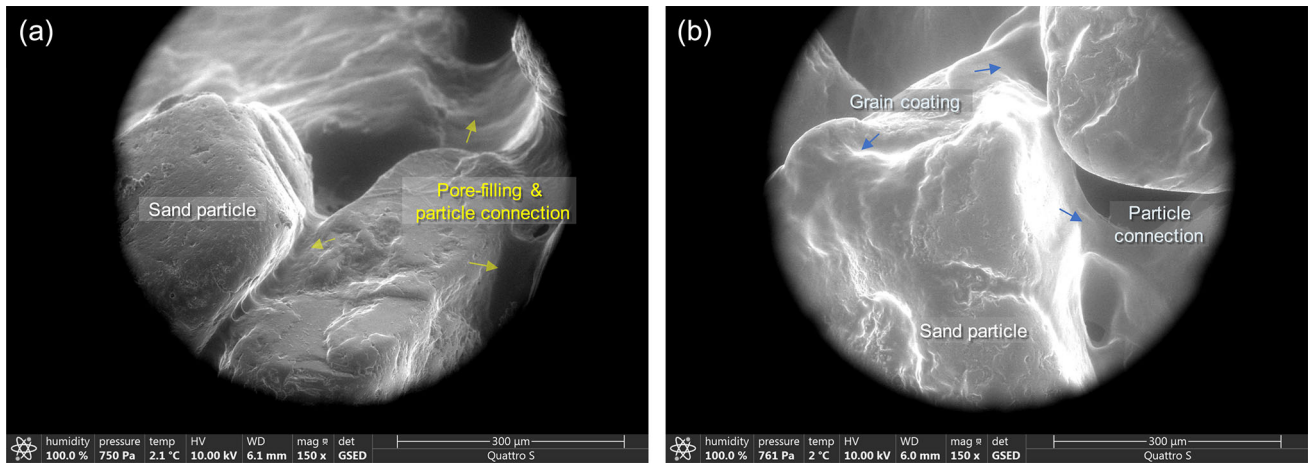


Fig. 12 ESEM images of biopolymer-treated soil specimens (magnification = 150x): **a** viscous-type XG; **b** gelation-type CrXG

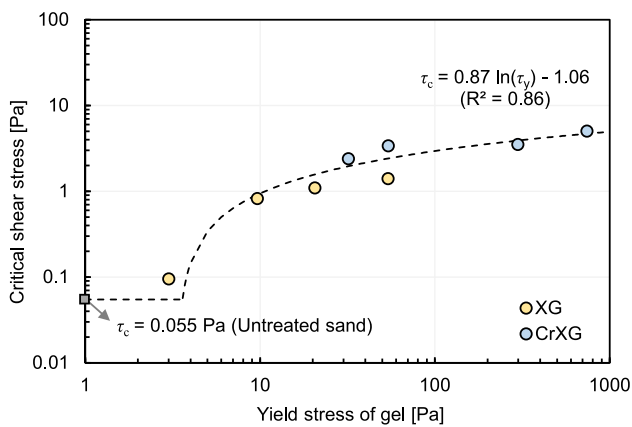


Fig. 13 Correlation between critical shear stress of sand treated with viscous gel-type biopolymers and yield stress of gel

resistance in EFA tests, could not be evaluated; however, it is anticipated that CX25(48 h) would likely result in a lower scour depth compared to other biopolymer treatments.

It should be noted that there are certain limitations. The scour predictions assume an ideal scenario with uniformly distributed biopolymers in a 1-m depth layer and no performance degradation over time. In practice, these predictions must account for in-situ mixing heterogeneity and

long-term durability. Although the host soil used in this study closely resembles *Seomjingang* Riverbed soil, characterized by low fine content (< 1%) and poorly graded coarse particles [85], future studies should evaluate the erosion resistance of CrXG-treated soils using natural riverbed materials for more accurate field application assessments.

4.3 Implementation and limitations

4.3.1 Technical and environmental considerations for CrXG applications

Potential applications of CrXG treatment in sandy soils primarily focus on erosion protection around riverbeds, slopes, embankments, bridge abutments, and culverts. For reinforcing surfaces, CrXG-soil composite can be applied through compaction or pressurized spraying methods. Studies on XG-based biopolymers have highlighted the importance of achieving homogeneity in biopolymer-soil mixtures, which is critical for both compaction and pressurized spraying applications [48, 74]. Monitoring mixture uniformity and strength over time is essential to ensure effective field application of CrXG treatment. In pressurized spraying, the time-dependent flow properties of CrXG

Table 4 Critical shear stress of viscous biopolymer-treated soil specimens and rheological yield stress of its gel

Biopolymer	Xanthan gum (XG)				Cr ³⁺ -crosslinked xanthan gum (CrXG)			
	X12	X25	X50	X100	CX12	CX25	CX50	CX100
Specimen	X12	X25	X50	X100	CX12	CX25	CX50	CX100
m_b/m_s [%]	0.125	0.25	0.5	1	0.125	0.25	0.5	1
Critical shear stress [Pa]	0.10	0.82	1.10	1.40	2.41	3.40	3.52	5.03
m_b/m_w [%]	0.675	1.25	2.5	5	0.675	1.25	2.5	5
Yield stress of gel [Pa]	3	10	21	54	32	54	298	741

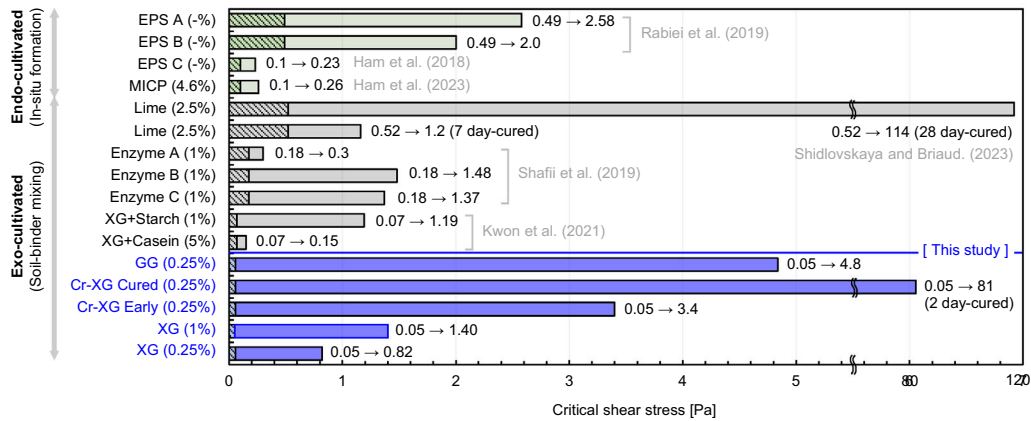


Fig. 14 Comparison of improved critical shear stress of sand stabilized using bio-based approaches. EPS A, B, and C were produced by the inoculation of *Calothrix*, *Nostoc*, and *Leuconostoc mesenteroides*, respectively. Enzyme A, B, C denotes TerraZyme, Road Ferment, Urease, respectively [31, 32, 43, 70, 75, 77]. The hatched area denotes the τ_c value associated with each untreated sandy soil

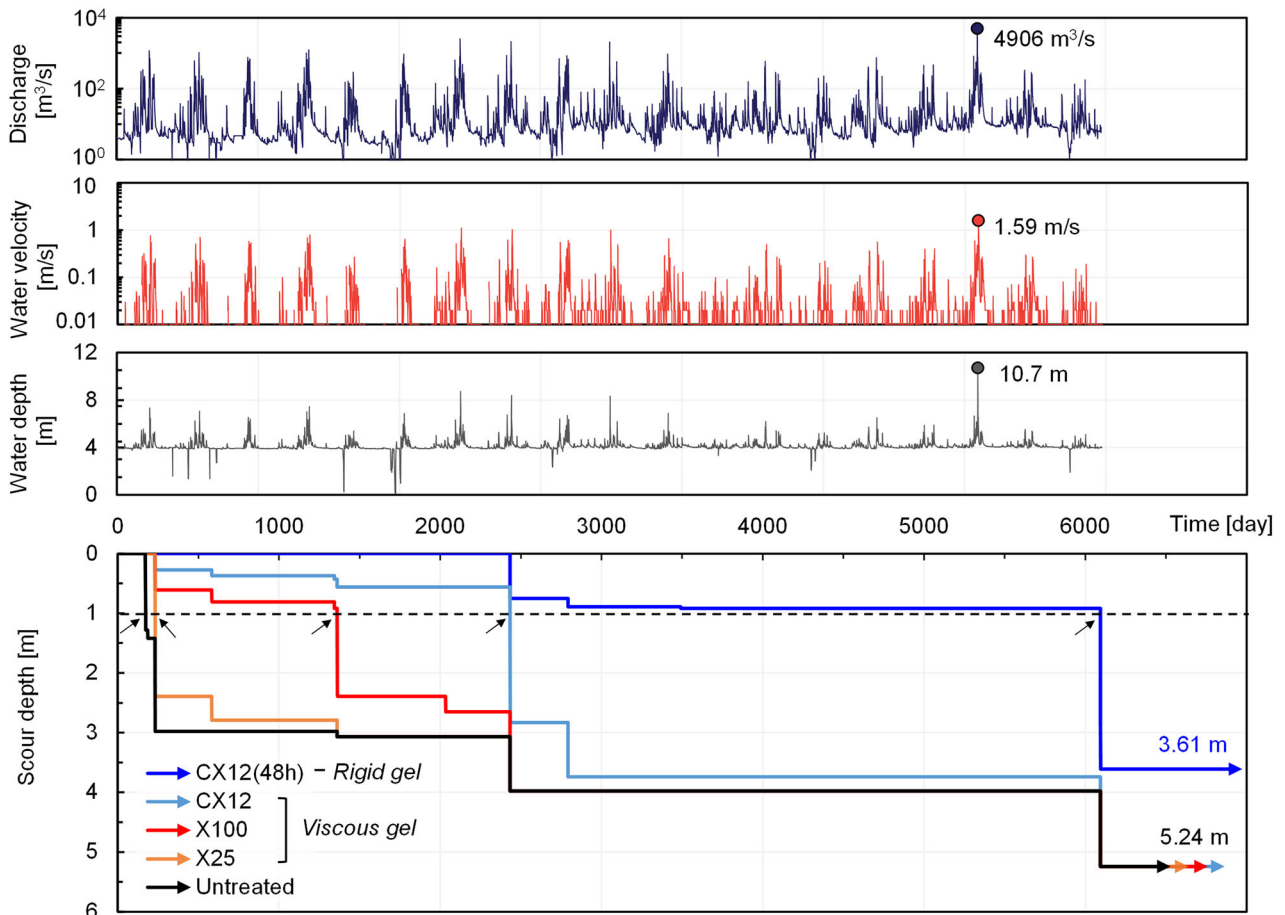


Fig. 15 The scouring depth predicted by SRICOS over 16 years with flow variations in the *Seomjingang* River

gel must also be carefully managed, as they impact workability like pumping efficiency and adhesion [55].

For erosion protection around interfaces or within soil structures, CrXG-soil composite can serve as backfill material around culverts or pipelines through in-situ

mixing and compaction. Pressurized injection methods, akin to those used in chemical grouting, may be used for rapid reinforcement in situations like embankment leaks or voids. The shear-thinning behavior of early stage CrXG gel allows it to penetrate pore spaces and fill cavities in sandy

soils effectively, with injectability influenced by both injection pressure and gel concentration [50]. Achieving gel saturation within pores is crucial for optimal erosion mitigation performance in these applications.

It is worth noting, however, that the effectiveness of CrXG treatment may be limited in clayey or marine soils. The anionically charged surfaces of clay particles can attract Cr^{3+} cations, creating competition between the XG hydrogel side chains and clay surfaces for Cr^{3+} in the presence of water [30]. This competition can disrupt the crosslinking-induced gelation process between XG and Cr^{3+} , resulting in a reduced crosslinking rate and density [69], which ultimately diminishes the strengthening effect in clay-rich environments [3]. Similar interference has been reported in other cation-polymer systems, such as chitosan and polyacrylamide [41, 69]. Consequently, while Cr^{3+} -crosslinked XG can improve erosion resistance in clayey or marine soils relative to untreated conditions, its performance may not match the level of efficacy achieved in sandy soils.

Additionally, to facilitate the above field applications, further in-depth research is required to assess the environmental impact of Cr^{3+} , particularly its leaching behavior under soil–water conditions. Cr^{3+} , the most stable and naturally occurring form of chromium, plays a vital role in metabolic functions [66] and is widely used due to its lower toxicity and limited water solubility compared to Cr^{6+} [4]. Nevertheless, chromium nitrate, used in this study, is noted in the Material Safety Data Sheet (MSDS, ThermoFisher Scientific) for its potential to cause long-term adverse effects in riverine ecosystems. Although the oxidation of Cr^{3+} to Cr^{6+} is infrequent in natural soil and aquatic environment [2, 28], prolonged water exposure may lead to the leaching of Cr^{3+} ions crosslinked within polymer network, posing risks to sensitive riparian zones. Consequently, further investigation into the leaching and sorption characteristics of Cr^{3+} in CrXG-soil composite is necessary. Based on these insights, implementing effective control and management strategies will be critical to minimize environmental risks associated with CrXG applications in soil stabilization.

4.3.2 Economic feasibility

To evaluate the economic feasibility of CrXG soil stabilization for erosion control, a comparative cost analysis was conducted against conventional methods. Commercial chemical grout, such as acrylic- and silicate-based solutions, range in cost from US\$ 2/m³ to US\$ 72/m³ [39]. In contrast, a 0.2-m thick reinforced soil layer using hydrated lime (at 2% to soil mass) incurs a cost of approximately US\$ 10/m² [77]. Materials required for MICP, including microorganisms, urea, and reagents, range from US\$ 0.5/

m³ to US\$ 9/m³, with total implementation costs from US\$ 75/m³ to US\$ 500/m³ [21]. Enzyme treatment, following a process similar to lime stabilization, have material costs of US\$ 1.6/m², totaling US\$ 11.6/m² [77]. For CrXG treatment, assuming a surface protection layer using a 0.2-m thick reinforced soil (m_b/m_s of 0.25%), the estimated material cost (excluding installation) is US\$ 3.3 for the treatment of 300 kg of soil based on unit prices of XG, $\text{Cr}(\text{NO}_3)_3$, and NaCl (Table S2) [79]. Following an in-situ mixing approach similar to lime stabilization, the total cost for CrXG treatment is estimated at US\$ 13.3/m². With further advances in production scalability and raw materials purity control [16], CrXG treatment has the potential to become a competitive option when compared to other bio-based materials, such as MICP (US\$ 0.5–9/m³) as well as traditional erosion control measures like filled sandbags [25]. While this study suggests that CrXG treatment could offer an effective and cost-conscious approach to mitigating surface erosion, a large-scale pilot study remains essential to fully assess its feasibility in terms of construction efficiency, equipment requirements, and post-construction maintenance costs.

5 Conclusions

This study investigated the impact of biopolymers on the erosion resistance of sandy soil under flowing water, focusing on how different biopolymer gel states influence erosion resistance. Three types of biopolymers: non-gelling viscous type (XG), cation crosslinking-induced gelation type (CrXG), and high-temperature thermogelation type (GG), with biopolymer content ranging from 0.125 to 1% by soil mass. CrXG-treated sand specimens were prepared under two conditions one at an early stage (< 6 h) and the other after 48 h of curing to account for the time-dependent gelation of CrXG. The study utilized an erosion function apparatus (EFA) with P-wave monitoring, rheological yield stress measurements, and ESEM observations. Additionally, SRICOS software was used to predict pier scour depth based on a 19-year hydrograph of a Korean stream. Key conclusions from this study are as follows:

XG, CrXG, and GG at m_b/m_s ranging from 0.125 to 1% improved erosion resistance of sand. Improvement efficiency followed the order: XG < early stage CrXG < GG < 48-h cured CrXG at equivalent m_b/m_s conditions, with greater erosion mitigation observed at higher m_b/m_s levels. Adding 0.25% CrXG to the soil increased τ_c by 62-fold and v_c by ninefold within 6 h. After 48 h of curing, Cr^{3+} crosslinking converted the gel from a viscous to a rigid state, which further enhanced τ_c

and shifted the soil erosion category from ‘very high erodibility’ to ‘low erodibility’.

A strong correlation was observed between the τ_c of sand treated with viscous-type biopolymer and the rheological τ_y of the hydrogel, suggesting that the viscous-type biopolymer hydrogel (XG and early stage CrXG) acts as a damper by dissipating erosional energy. However, under higher flow conditions, it loses this damping effect, allowing particle detachment to initiate. Meanwhile, gelation-type biopolymer hydrogel (48-h-cured CrXG and GG), provides intergranular bonding effect with grain coating to sand in a rigid gel state, increasing energy required to break interparticle bonding and bring the eroded particles to suspension.

Pier scour depth prediction using SRICOS showed that biopolymer treatments effectively mitigated scouring, with XG treatment extending the time to reach a 1-m scour depth by up to 7.9 times, depending on the dosage. CrXG treatment showed superior performance, delaying the 1-m scour depth by up to 35 times. After 19 years, the final scour depth was 5.24 m for untreated and viscous-type biopolymer treated soils, while gelation-type biopolymer treated soils reduced scour depth by 31% to 3.61 m, even under extreme flood conditions.

While this study focused on a specific soil type, the findings elucidate the influence of different gel states on surface erosion behavior of sand, the relationship between rheological yield stress and erosion resistance, and the efficiency and competitiveness of cation-crosslinked gelation biopolymer treatment. Further research is needed to evaluate CrXG’s efficacy in natural soils, particularly clay-rich soil, and to investigate environmental implications of Cr^{3+} leaching under soil–water conditions. Additionally, large-scale pilot studies are recommended to assess long-term durability, construction efficiency, and to refine optimal configurations and design parameters for practical field applications.

Supplementary Information The online version contains supplementary material available at <https://doi.org/10.1007/s11440-025-02577-z>.

Acknowledgements This research was supported by the National Research Foundation of Korea (NRF) grant (No. 2023R1A2C300559611) funded by the Korea government (MSIT). The first author was also supported by the Nuclear Research and Development Program of NRF grant (No. 2021M2E3A2041351) funded by the Korean Government (Ministry of Science and ICT, MSIT).

Author Contribution M.L: Conceptualization, Methodology, Investigation, Visualization, Validation, Writing – original draft. I.C: Supervision, Validation, Writing – review & editing. G.C.C: Resources, Supervision, Project administration, Funding acquisition, Writing – review & editing.

Funding Open Access funding enabled and organized by KAIST.

Availability of data and materials No datasets were generated or analysed during the current study.

Declarations

Conflict of interest The authors declare no competing interests.

Open Access This article is licensed under a Creative Commons Attribution 4.0 International License, which permits use, sharing, adaptation, distribution and reproduction in any medium or format, as long as you give appropriate credit to the original author(s) and the source, provide a link to the Creative Commons licence, and indicate if changes were made. The images or other third party material in this article are included in the article’s Creative Commons licence, unless indicated otherwise in a credit line to the material. If material is not included in the article’s Creative Commons licence and your intended use is not permitted by statutory regulation or exceeds the permitted use, you will need to obtain permission directly from the copyright holder. To view a copy of this licence, visit <http://creativecommons.org/licenses/by/4.0/>.

References

1. Abt SR, Johnson TL (1991) Riprap design for overtopping flow. *J Hydraul Eng* 117(8):959–972. [https://doi.org/10.1061/\(ASCE\)0733-9429\(1991\)117:8\(959\)](https://doi.org/10.1061/(ASCE)0733-9429(1991)117:8(959))
2. Apte AD et al (2006) Extent of oxidation of Cr(III) to Cr(VI) under various conditions pertaining to natural environment. *J Hazard Mater* 128(2–3):164–174. <https://doi.org/10.1016/j.jhazmat.2005.07.057>
3. Bang J-U et al (2024) Effects of soil composition and curing conditions on the strength and durability of Cr³⁺-crosslinked biopolymer-soil composites. *Const Build Mater* 449:138440
4. Baruthio F (1992) Toxic effects of chromium and its compounds. *Biol Trace Elem Res* 32(1):145–153. <https://doi.org/10.1007/BF02784599>
5. Biamino S, Badini C (2004) Combustion synthesis of lanthanum chromite starting from water solutions: investigation of process mechanism by DTA–TGA–MS. *J Eur Ceram Soc* 24(10–11):3021–3034. <https://doi.org/10.1016/j.jeurceramsoc.2003.10.005>
6. Briaud J-L (2008) Case histories in soil and rock erosion: Woodrow wilson bridge, brazos river meander, normandy cliffs, and new orleans levees. *J Geotechn Geoenviron Eng* 134(10):1425–1447. [https://doi.org/10.1061/\(ASCE\)1090-0241\(2008\)134:10\(1425\)](https://doi.org/10.1061/(ASCE)1090-0241(2008)134:10(1425))
7. Briaud J-L et al (2008) Levee erosion by overtopping in New Orleans during the Katrina Hurricane. *J Geotechn Geoenviron Eng* 134(5):618–632. [https://doi.org/10.1061/\(ASCE\)1090-0241\(2008\)134:5\(618\)](https://doi.org/10.1061/(ASCE)1090-0241(2008)134:5(618))
8. Briaud J-L et al (1999) SRICOS: Prediction of scour rate in cohesive soils at bridge piers. *J Geotechn Geoenviron Eng* 125(4):237–246. [https://doi.org/10.1061/\(ASCE\)1090-0241\(1999\)125:4\(237\)](https://doi.org/10.1061/(ASCE)1090-0241(1999)125:4(237))
9. Briaud J et al (2001) Multiflood and multilayer method for scour rate prediction at bridge piers. *J Geotech Geoenviron Eng* 127(2):114–125. [https://doi.org/10.1061/\(ASCE\)1090-0241\(2001\)127:2\(114\)](https://doi.org/10.1061/(ASCE)1090-0241(2001)127:2(114))
10. Briaud JL et al (2001) Erosion function apparatus for scour rate predictions. *J Geotech Geoenviron Eng* 127(2):105–113. [https://doi.org/10.1061/\(ASCE\)1090-0241\(2001\)127:2\(105\)](https://doi.org/10.1061/(ASCE)1090-0241(2001)127:2(105))

11. Cabalar AF et al (2017) Effects of xanthan gum biopolymer on the permeability, odometer, unconfined compressive and triaxial shear behavior of a sand. *Soil Mech Found Eng* 54(5):356–361. <https://doi.org/10.1007/s11204-017-9481-1>
12. Chang I, Cho G-C (2019) Shear strength behavior and parameters of microbial gellan gum-treated soils: from sand to clay. *Acta Geotech* 14(2):361–375. <https://doi.org/10.1007/s11440-018-0641-x>
13. Chang I et al (2016) Geotechnical engineering behaviors of gellan gum biopolymer treated sand. *Can Geotech J* 53(10):1658–1670. <https://doi.org/10.1139/cgj-2015-0475>
14. Chang I et al (2015) Effects of xanthan gum biopolymer on soil strengthening. *Const Build Mater* 74:65–72. <https://doi.org/10.1016/j.conbuildmat.2014.10.026>
15. Chang I et al (2021) Effect of pore-fluid chemistry on the undrained shear strength of xanthan gum biopolymer-treated clays. *J Geotech Geoenviron Eng* 147(11):06021013. [https://doi.org/10.1061/\(ASCE\)GT.1943-5606.0002652](https://doi.org/10.1061/(ASCE)GT.1943-5606.0002652)
16. Chang I et al (2020) Review on biopolymer-based soil treatment (BPST) technology in geotechnical engineering practices. *Trans Geotech* 24:100385. <https://doi.org/10.1016/j.trgeo.2020.100385>
17. Chen C et al (2019) The drying effect on xanthan gum biopolymer treated sandy soil shear strength. *Const Build Mater* 197:271–279. <https://doi.org/10.1016/j.conbuildmat.2018.11.120>
18. Chen J et al (2021) Effects of bacterial activity on the saturated hydraulic conductivity of remolded loess. *Eng Geol* 287:106101. <https://doi.org/10.1016/j.enggeo.2021.106101>
19. Clarà Saracho A et al (2021) Flume study on the effects of microbial induced calcium carbonate precipitation (MICP) on the erosional behaviour of fine sand. *Géotechnique* 71(12):1135–1149. <https://doi.org/10.1680/jgeot.19.p.350>
20. DeJong JT et al (2010) Bio-mediated soil improvement. *Ecol Eng* 36(2):197–210. <https://doi.org/10.1016/j.ecoleng.2008.12.029>
21. DeJong JT et al (2013) Biogeochemical processes and geotechnical applications: progress, opportunities and challenges. *Géotechnique* 63(4):287–301. <https://doi.org/10.1680/geot.SIP13.P.017>
22. Dogan M et al (2013) Steady, dynamic, creep, and recovery analysis of ice cream mixes added with different concentrations of xanthan gum. *Food Bioproc Tech* 6:1420–1433. <https://doi.org/10.1007/s11947-012-0872-z>
23. Dolan D et al (1998) Effects of pH and Shear on the Gelation of a Cr (III)-Xanthan System. *SPE Prod Facil* 13(02):97–103. <https://doi.org/10.2118/25454-PA>
24. Du Y-J et al (2014) Effect of acid rain pH on leaching behavior of cement stabilized lead-contaminated soil. *J Hazard Mater* 271:131–140. <https://doi.org/10.1016/j.jhazmat.2014.02.002>
25. Dubey AA et al (2022) Biopolymer-biocement composite treatment for stabilisation of soil against both current and wave erosion. *Acta Geotech* 17(12):5391–5410. <https://doi.org/10.1007/s11440-022-01536-2>
26. Dubey AA et al (2023) Rheological properties of xanthan-gum solutions and their role in improving river embankments. *Geotechn Geol Eng*. <https://doi.org/10.1007/s10706-023-02678-0>
27. Dzuy NQ, Boger DV (1985) Direct yield stress measurement with the vane method. *J Rheol* 29(3):335–347. <https://doi.org/10.1122/1.549794>
28. Eary LE, Rai D (1987) Kinetics of chromium(III) oxidation to chromium(VI) by reaction with manganese dioxide. *Environ Sci Technol* 21(12):1187–1193. <https://doi.org/10.1021/es00165a005>
29. Gales JR et al (1994) Equilibrium swelling and syneresis properties of Xanthan Gum/Cr(III) Gels. *SPE Adv Techn Series* 2(02):190–198. <https://doi.org/10.2118/17328-pa>
30. Garver, F., et al. (1989). The competition for chromium between xanthan biopolymer and resident clays in sandstones. SPE Annual Technical Conference and Exhibition, OnePetro.
31. Ham S-M et al (2018) Improvement of surface erosion resistance of sand by microbial biopolymer formation. *J Geotechn Geoenviron Eng* 144(7):06018004. [https://doi.org/10.1061/\(ASCE\)GT.1943-5606.0001900](https://doi.org/10.1061/(ASCE)GT.1943-5606.0001900)
32. Ham S-M et al (2023) Surface erosion of MICP-treated sands: erosion function apparatus tests and CFD-DEM bonding model. *Geomech. Eng.* 33(2):133–140
33. Ham S et al (2016) Ultrasonic P-wave reflection monitoring of soil erosion for erosion function apparatus. *Geotech Test J* 39(2):301–314. <https://doi.org/10.1520/GTJ20150040>
34. Hamdan N, Kavazanjian E Jr (2016) Enzyme-induced carbonate mineral precipitation for fugitive dust control. *Géotechnique* 66(7):546–555
35. Hey RD (1979) Flow resistance in gravel-bed rivers. *J Hydraul Div* 105(4):365–379. <https://doi.org/10.1061/JYCEAJ.0005178>
36. Hunt JA et al (1989) A study of Cr (III)-polyacrylamide reaction kinetics by equilibrium dialysis. *AIChE J* 35(2):250–258. <https://doi.org/10.1002/aic.690350209>
37. Im, J. (2020). Polysaccharide biopolymers in sands: properties and behaviors. Department of Civil and Environmental Engineering. Daejeon, South Korea, Korea Advanced Institute of Science and Technology (KAIST). **Ph. D. Dissertation:** 1–92.
38. Indraratna B et al (2008) Predicting the erosion rate of chemically treated soil using a process simulation apparatus for internal crack erosion. *J Geotechn Geoenviron Eng* 134(6):837–844. [https://doi.org/10.1061/\(ASCE\)1090-0241\(2008\)134:6\(837\)](https://doi.org/10.1061/(ASCE)1090-0241(2008)134:6(837))
39. Ivanov V, Chu J (2008) Applications of microorganisms to geotechnical engineering for bioclogging and biocementation of soil in situ. *Rev Environ Sci Biotechnol* 7(2):139–153. <https://doi.org/10.1007/s11157-007-9126-3>
40. Hanson JG, Cook KR (2004) Apparatus, test procedures, and analytical methods to measure soil erodibility in situ. *Appl Eng Agric.* 20(4):455–462
41. Kabiri K et al (2009) Chitosan-modified nanoclay–poly (AMPS) nanocomposite hydrogels with improved gel strength. *Polym Int* 58(11):1252–1259
42. Kang W et al (2021) Erosion resistance performance of surface-reinforced levees using novel biopolymers investigated via real-scale overtopping experiments. *Water* 13(18):2482. <https://doi.org/10.3390/w13182482>
43. Kwon Y-M et al (2021) Surface erosion behavior of biopolymer-treated river sand. *Geomechan Eng.* 25(1):49–58
44. Kwon Y-M et al (2020) Surface-erosion behaviour of biopolymer-treated soils assessed by EFA. *Géotechnique Letters* 10(2):1–7. <https://doi.org/10.1680/jgele.19.00106>
45. Kwon Y-M et al (2023) Xanthan gum biopolymer-based soil treatment as a construction material to mitigate internal erosion of earthen embankment: A field-scale. *Const Build Mater* 389:131716. <https://doi.org/10.1016/j.conbuildmat.2023.131716>
46. Lagasse, P. F., et al. (1995). Stream stability at highway structures, United States. Federal Highway Administration. Office of Technology Applications.
47. Lee M et al (2023) Advanced biopolymer-based soil strengthening binder with trivalent chromium–xanthan gum crosslinking for wet strength and durability enhancement. *J Mater Civ Eng* 35(10):04023360. <https://doi.org/10.1061/JMCEE7/MTENG-16123>
48. Lee M et al (2023) Alkaline induced-cation crosslinking biopolymer soil treatment and field implementation for slope surface protection. *Geomech Eng* 33(1):29–40
49. Lee M et al (2023) Strengthening and permeability control in sand using Cr3+-crosslinked xanthan gum biopolymer treatment. *Trans Geotech* 43:101122. <https://doi.org/10.1016/j.trgeo.2023.101122>
50. Lee M et al (2021) Evaluation of Injection capabilities of a biopolymer-based grout material. *Geomech Eng.* 25(1):31–40

51. Lee M et al (2021) Interfacial shearing behavior along xanthan gum biopolymer-treated sand and solid interfaces and its meaning in geotechnical engineering aspects. *Appl Sci* 11(1):139. <https://doi.org/10.3390/app11010139>
52. Léonard J, Richard G (2004) Estimation of runoff critical shear stress for soil erosion from soil shear strength. *CATENA* 57(3):233–249. <https://doi.org/10.1016/j.catena.2003.11.007>
53. Li H et al (2019) Design and construction application of concrete canvas for slope protection. *Powder Technol* 344:937–946. <https://doi.org/10.1016/j.powtec.2018.12.075>
54. Liang Y et al (2021) Experimental investigation on hole erosion behaviors of chemical stabilizer treated soil. *J Hydrol* 594:125647. <https://doi.org/10.1016/j.jhydrol.2020.125647>
55. Liu G et al (2020) Rheological properties of fresh concrete and its application on shotcrete. *Const Build Mater* 243:118180. <https://doi.org/10.1016/j.conbuildmat.2020.118180>
56. Liu Y et al (2023) An experimental investigation of wind erosion resistance of desert sand cemented by soybean-urease induced carbonate precipitation. *Geoderma* 429:116231. <https://doi.org/10.1016/j.geoderma.2022.116231>
57. Losini AE et al (2021) Natural additives and biopolymers for raw earth construction stabilization—a review. *Const Build Mater* 304:124507. <https://doi.org/10.1016/j.conbuildmat.2021.124507>
58. Marudova-Zsivanovits M et al (2007) Rheological investigation of xanthan gum–chromium gelation and its relation to enhanced oil recovery. *J Appl Polym Sci* 103(1):160–166. <https://doi.org/10.1002/app.25025>
59. McLean, J. E. (1992). Behavior of metals in soils. In *Ground water issue*, Technology Innovation Office, Office of Solid Waste and Emergency Response, U.S. Environmental Protection Agency, United States.
60. Montoya BM, DeJong JT (2015) Stress-strain behavior of sands cemented by microbially induced calcite precipitation. *Journal of Geotechnical and Geoenviron Eng* 141(6):04015019. [https://doi.org/10.1061/\(ASCE\)GT.1943-5606.0001302](https://doi.org/10.1061/(ASCE)GT.1943-5606.0001302)
61. Moody LF (1944) Friction factors for pipe flow. *Trans Am Soc Mech Eng* 66:671–684. <https://doi.org/10.1115/1.4018140>
62. National Institute of Environmental Research (NIER) Water environment information system. water.nier.go.kr, 2023 (accessed 25 December 2023).
63. Noh D-H et al (2021) Effect of soft viscoelastic biopolymer on the undrained shear behavior of loose sands. *J Geotech Geoenviron Eng* 147(8):04021072. [https://doi.org/10.1061/\(ASCE\)GT.1943-5606.0002582](https://doi.org/10.1061/(ASCE)GT.1943-5606.0002582)
64. Nolte H et al (1992) Gelation of xanthan with trivalent metal ions. *Carbohydr Polym* 18(4):243–251. [https://doi.org/10.1016/0144-8617\(92\)90089-9](https://doi.org/10.1016/0144-8617(92)90089-9)
65. Park C et al (2021) Record-breaking summer rainfall in South Korea in 2020: Synoptic characteristics and the role of large-scale circulations. *Mon Weather Rev* 149(9):3085–3100. <https://doi.org/10.1175/MWR-D-21-0051.1>
66. Pechova A, Pavlata L (2007) Chromium as an essential nutrient: a review. *Vet medi* 52(1):1
67. Philippova OE et al (2016) Structure and rheology of solutions and gels of stiff polyelectrolyte at high salt concentration. *Macromol* 49(16):6031–6040. <https://doi.org/10.1021/acs.macromol.6b01392>
68. Pintelon TR et al (2012) The effect of biofilm permeability on bio-clogging of porous media. *Biotechnol Bioeng* 109(4):1031–1042. <https://doi.org/10.1002/bit.24381>
69. Pu WF et al (2016) Gelation performance of poly (ethylene imine) crosslinking polymer–layered silicate nanocomposite gel system for potential water-shutoff use in high-temperature reservoirs. *J Appl Polym Sci*. <https://doi.org/10.1002/app.44243>
70. Rabiei A et al (2022) Reducing hydraulic erosion of surficial sand layer by inoculation of cyanobacteria. *Proc Inst Civ Eng Ground Improv*. 175(3):209–221
71. Renjith R et al (2021) Optimization of fly ash based soil stabilization using secondary admixtures for sustainable road construction. *J Clean Prod* 294:126264. <https://doi.org/10.1016/j.jclepro.2021.126264>
72. Richard FC, Bourg AC (1991) Aqueous geochemistry of chromium: a review. *Water Res* 25(7):807–816
73. Schulze K et al (2005) Simulating river flow velocity on global scale. *Adv Geosci* 5:133–136. <https://doi.org/10.5194/adgeo-5-133-2005>
74. Seo S et al (2021) Site application of biopolymer-based soil treatment (BPST) for slope surface protection: in-situ wet-spraying method and strengthening effect verification. *Const Build Mater* 307:124983. <https://doi.org/10.1016/j.conbuildmat.2021.124983>
75. Shafii I et al (2019) Investigation into the effect of enzymes on the erodibility of a low-plasticity silt and a silty sand by EFA testing. *J Geotech Geoenviron Eng* 145(3):04019001. [https://doi.org/10.1061/\(ASCE\)GT.1943-5606.0002019](https://doi.org/10.1061/(ASCE)GT.1943-5606.0002019)
76. Shibaev AV et al (2020) pH-dependent gelation of a stiff anionic polysaccharide in the presence of metal ions. *Polym* 12(4):868. <https://doi.org/10.3390/polym12040868>
77. Shidlovskaya A, Briaud J-L (2023) Erosion mitigation using grass, riprap, lime, and enzymes. *J Geotech Geoenviron Eng* 149(4):04023011. [https://doi.org/10.1061/\(ASCE\)GT.1943-5606.0002918](https://doi.org/10.1061/(ASCE)GT.1943-5606.0002918)
78. Shirole AM, Holt RC (1991) Planning for a comprehensive bridge safety assurance program. *Transp Res Rec* 1290:39–50
79. Soltaninejad A et al (2022) Biorefinery for efficient xanthan gum, ethanol, and biogas production from potato crop residues. *Biomass Bioenergy* 158:106354. <https://doi.org/10.1016/j.biombioe.2022.106354>
80. Song K-W et al (2006) Rheology of concentrated xanthan gum solutions: Steady shear flow behavior. *Fibers Polymers* 7(2):129–138
81. Su H et al (2021) Experimental and numerical study on stability performance of new ecological slope protection using bolt-hinge anchored block. *Ecol Eng* 172:106409. <https://doi.org/10.1016/j.ecoleng.2021.106409>
82. Valela C et al (2022) Novel riprap structure for improved bridge pier scour protection. *J Hydraul Eng* 148(3):04022002. [https://doi.org/10.1061/\(ASCE\)HY.1943-7900.0001967](https://doi.org/10.1061/(ASCE)HY.1943-7900.0001967)
83. Vishweshwaran M, Sujatha ER (2021) Experimental investigation and numerical modeling of a cross-linked biopolymer stabilized soil. *Arab J Geosci* 14:1–16. <https://doi.org/10.1007/s12517-021-08260-3>
84. Wan C, Fell R (2004) Laboratory tests on the rate of piping erosion of soils in embankment dams. *Geotech Test J* 27(3):295–303. <https://doi.org/10.1520/GTJ11903>
85. You H-S et al (2000) Fluvial deposits distributed along the Seomjin River. *J Korean Earth Sci Soc* 21(2):174–187
86. Zhuang X et al (2018) Spatial distribution of sheet flow velocity along slope under simulated rainfall conditions. *Geoderma* 321:1–7. <https://doi.org/10.1016/j.geoderma.2018.01.036>
87. Zuazo VHD, Pleguezuelo CRR (2009) Soil-erosion and runoff prevention by plant covers: a review. *Agron Sustain Dev* 28(1):785–811. <https://doi.org/10.1051/agro:2007062>

Publisher's Note Springer Nature remains neutral with regard to jurisdictional claims in published maps and institutional affiliations.